Second International Symposium on Marine Propulsors
smp'11, Hamburg, Germany, June 2011

On the Capability of Multiphase RANS Codes to Predict Cavitation Erosion

Ziru Li[1], Tom Van Terwisga[1,2]

[1]Delft University of Technology, The Netherlands
[2]Maritime Research Institute Netherlands (MARIN)

ABSTRACT

The reliability of the prediction of cavitation nuisance, such as cavitation erosion, has been extensively investigated in the last decades. Today, there are still serious debates whether a certain type of cavitation is erosive or not. This paper addresses the question whether the conditions for erosive cavitation can be predicted from unsteady two-phase RANS codes without the necessity to compute the details of the actual collapse.

To investigate this question, numerical studies with the RANS code FLUENT are conducted on the frequently-used NACA0015 hydrofoil and on a NACA0018-45 hydrofoil where experimental data is available for similar studies. A stronger adverse pressure gradient near the trailing edge for the NACA0018-45 hydrofoil is observed, implying potentially more intensive unsteady dynamics and a correspondingly higher erosion risk. It is concluded that a realistic dynamic behavior of break up is only obtained after attenuating the eddy viscosity in regions of higher vapor volume fraction. Finally, a qualitative analysis of the cavitation erosion risk on the 3D NACA0015 hydrofoil is made to assess the capability of a multiphase RANS code to predict the risk of cavitation erosion.

Keywords

Two-phase RANS, unsteady cavitation, Reboud's correction, cavitation erosion

1 INTRODUCTION

The prediction of cavitation nuisance is a necessary condition for the successful optimization of propulsors and propulsor-aftbody configurations. The reason is that efficiency considerations and cavitation nuisance considerations lead to counteracting measures in the propeller design (Ligtelijn 2010). So if cavitation nuisance consisting of hull vibrations and cavitation erosion is not predicted sufficiently well, the value of the attainable efficiency is highly uncertain. The issue of the reliability of cavitation nuisance predictions is an old one. Several ITTC specialist committees on cavitation have addressed this question, but modern two-phase unsteady RANS codes seem to offer an improvement in the capability of predicting this nuisance. But do they really? This paper sets out to explore an answer to this question with a thorough study on a frequently-used NACA-0015 hydrofoil and a NACA0018-45 hydrofoil, where experimental data is available for similar studies.

Van Terwisga et al (2009) hypothesize that the erosive action from cavitation is largely caused by the acoustic shock waves that are released upon collapse of a focused cavity. This hypothesis builds further on the fundamental work done on cavitation erosion by Bark et al (2004). It is suggested here that the focusing of potential energy in the cavity is occurring through large scale vortices produced in the break-up region of sheet cavitation. This paper focuses on the question whether the conditions for erosive cavitation can be predicted from unsteady two-phase RANS computations without computing the details of the actual collapse. This would then justify a focus on modeling only the large scale cavity dynamics correctly.

At first, the flow characteristics under the non-cavitating condition are investigated on both hydrofoils by the RANS code FLUENT. These results are compared with the results from XFOIL (Mark & Harold 2001), including viscous effects. It is interesting to note that in the pressure distribution of the NACA0018-45 hydrofoil, there is a characteristic pressure gradient near the trailing edge, which is very different from the NACA0015 foil (see Fig.2). Consequently, stronger cavitation dynamics can be expected. Due to this more adverse pressure gradient, a larger separation zone is also observed near the trailing edge for the NACA0018-45 foil.

Subsequently, a specific cavitation regime characterized by relatively strong dynamic shedding ($\sigma = 1.0$) is investigated on both hydrofoils to examine the unsteady dynamics and to verify the above assumption. The results on the 2D NACA0015 hydrofoil with the FLUENT multiphase RANS code indicate that a realistic dynamic behavior of break-up of sheet cavitation is only obtained after attenuating the eddy viscosity in the cavity-liquid interface (Reboud et al 1998). A numerical investigation is conducted on the 2D NACA0015 hydrofoil to check whether numerical issues would affect the break-up phenomena. Some RANS results based on the VIRTUE Workshop by Li Daqing et al (2009), Oprea et al (2009)

and Hoekstra et al (2008) would give a comparison to verify these numerical uncertainty analyses.

The results on the 3D NACA0015 foil indicate that the most likely position for cavitation erosion to occur can be assessed from the URANS results but that criteria for a sound risk assessment are still lacking. Further research is demanded for a reliable prediction of the risk of the cavitation erosion.

2 NUMERICAL MODELS

2.1 Governing Equations

The governing equations for a two-phase flow are based on a single-fluid approach, regarding the mixture as one liquid. The flow field is solved for the mixture continuity and momentum equations,

$$\frac{\partial}{\partial t}(\rho_m) + \nabla \cdot (\rho_m \vec{v}) = \upsilon \tag{1}$$

$$\begin{aligned} &\frac{\partial}{\partial t}(\rho_m \vec{v}) + \nu \cdot (\rho_m \vec{v}\vec{v}) \\ &= -\nabla p + \nabla \cdot [\mu_m (\nabla \vec{v} + \nu \vec{v}\ )] + \rho_m \vec{g} + r \end{aligned} \tag{2}$$

Where the relationship between the mixture density ρ_m and the vapor volume fraction α is defined as:

$$\rho_m = \alpha \rho_v + (1-\alpha)\rho_l \tag{3}$$

Where subscripts m, v and l represent mixture, vapor and liquid phase, respectively.

2.2 Turbulence Modeling

The $SST\ k-\omega$ turbulence model is adopted in this study, which is a blending between the $k-\omega$ model in the near-wall region and the $k-\varepsilon$ model in the far field developed by Menter (1994). The refinements of the $k-\omega$ model and a blending function can make this model behave properly in both the near-wall and far-field zones. To improve the cavity dynamics in the simulation, a modification of the turbulent viscosity, μ_t, is applied following the idea of Reboud et al (1998).

$$\mu_t = f(\rho) C_\omega \frac{k}{\omega} \tag{4}$$

$$f(\rho) = \rho_v + \frac{(\rho_m - \rho_v)^n}{(\rho_l - \rho_v)^{n-1}}; \quad n \square \tag{5}$$

With a recommended exponent value $n = 10$, the turbulent viscosity in the region with higher vapor volume fraction is reduced to better simulate the re-entrant jet and shedding behavior.

2.3 Cavitation Modeling

The cavitation model adopted here is developed by Schnerr & Sauer (2001). The transport equation for the vapor volume fraction has the general form:

$$\frac{\partial}{\partial t}(\alpha \rho_v) + \nabla \cdot (\alpha \rho_v \vec{V}) = R_e - R_c \tag{6}$$

Where the source term R_e and R_c are connected to the evaporation and condensation of the vapor bubbles respectively, accounting for the mass transfer between the vapor and liquid phases in cavitation. The source terms are derived from the Rayleigh-Plesset equation and are defined as:

$$R_e = \frac{\rho_v \rho_l}{\rho_m} \alpha(1-\alpha) \frac{3}{\Re_B} \sqrt{\frac{2}{3} \frac{(P_v - P)}{\rho_l}}, \text{ when } P_v \geq P \tag{7}$$

$$R_c = \frac{\rho_v \rho_l}{\rho_m} \alpha(1-\alpha) \frac{3}{\Re_B} \sqrt{\frac{2}{3} \frac{(P - P_v)}{\rho_l}}, \text{ when } P_v \leq P \tag{8}$$

The bubble radius can be related to the vapor volume fraction α and the bubble number density n_b as follows:

$$\Re_B = \left(\frac{\alpha}{1-\alpha} \frac{3}{4\pi n_b}\right)^{\frac{1}{3}} \tag{9}$$

Where n_b is the only parameter to be provided as input for FLUENT with a default value of $1e+13$.

3 NUMERICAL RESULTS AND DISCUSSION

There are two hydrofoils to be calculated by the RANS code FLUENT. The first case to be studied is a NACA0015 hydrofoil at an angle of attack of 6 deg around the center of gravity $x/c = 0.3086$, with a chord length $c = 200mm$. This foil is chosen as the study case for the Virtue_WP4 Workshop. The size of the computational domain is $1400 \times 570mm$, extending 2 chord lengths ahead of the leading edge and 4 chord lengths behind the trailing edge. The adopted grid is the finest block-structured grid with 111,232 cells, consisting of an O-grid around the hydrofoil, embedded in an H-grid (12 blocks), as shown in Fig. 1 a). As an interest of the validation with the experimental data, a second case is chosen as a NACA0018-45 hydrofoil at an angle of attack of 5.8 deg around the center of gravity $x/c = 0.5$, with a chord length $c = 60mm$. The size of the computational domain is $4200 \times 80mm$, extending 2 chord lengths ahead of the leading edge and 4 chord lengths behind the trailing edge, and the dimension in y direction is set to be $80mm$ corresponding to the size of the cavitation tunnel. The grid is an O-H multi-block one with similar topology as the NACA0015 hydrofoil, shown in Fig.1 b).

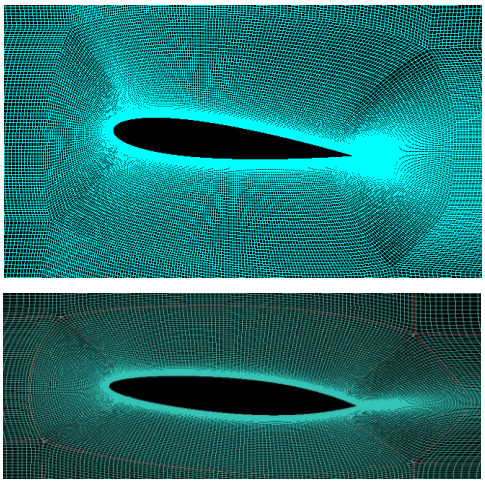

a)

b)

Figure 1: The mesh around the (a) NACA0015 hydrofoil; and (b) NACA0018-45 hydrofoil

Two conditions are calculated for both hydrofoils: a non-cavitating condition, and a cavitating condition at $\sigma = 1.0$ which is expected to be unsteady with cyclic shedding. A fully coupled solver is selected to solve the pressure and momentum equations, which can lead to a more robust calculation and faster convergence (ANSYS FLUENT Manual 2009). A velocity-inlet boundary condition is applied on the upstream inflow, and the vapor volume fraction is specified to equal zero. On the outlet boundary, a pressure-outlet boundary condition is used, where the cavitation number can be derived from the specified pressure at the outlet:

$$\sigma = \frac{p_{out} - p_v}{\rho U_0^2 / 2} \qquad (10)$$

The detailed boundary conditions and the physical properties of the flow for both cases are listed in Table 1. The discretization schemes adopt QUICK in space, PRESTO for pressure and first order implicit in time.

Table 1: Boundary conditions and flow properties

Boundary Conditions	NACA0015		NACA0018-45	
Velocity Inlet (m/s)	V=6		V=18.3	
Pressure Outlet(kPa)	20.9		168.9	
Turbulent Intensity (%)	1			
Turbulent Viscosity Ratio	10			
Foil	No-slip Wall			
Tunnel Wall	Slip Wall		No-slip Wall	
Flow Properties	Vapour	Liquid	Vapour	Liquid
Density (kg/m3)	0.023	998	0.01193	999.2267
Dynamic Viscosity(kg/ms)	9.95E-06	0.0011	9.56E-06	0.001175
Vapor Pressure (kPa)	2.97		1.578	

3.1 2D Non-cavitating Condition

Unlike the frequently-used NACA0015 hydrofoil, it is difficult to find the comparable wetted flow characteristics of the NACA018-45 hydrofoil, such as the pressure, lift and drag coefficients. Therefore, the XFOIL results including viscous effect are used to give a comparison with the flow characteristics predicted by FLUENT.

From the pressure vectors along the hydrofoils, it can be observed that much larger adverse pressure occur on the pressure side of the NACA0018-45 hydrofoil than the NACA0015 hydrofoil. Moreover, this observation is also confirmed by the results of pressure coefficient distribution along both hydrofoils, as shown in Fig. 2. Fig. 2 shows that the NACA0018-45 foil shows a much steeper adverse pressure gradient than the NACA0015 foil. As a consequence, a larger separation zone is observed near the trailing edge for the NACA0018-45 foil, as shown in Fig. 3. This steeper pressure gradient also implies that more intense dynamics can be expected in the unsteady cavitating flow.

It is also noted that the two different geometries show a different sensitivity to the computational domain. There are no big differences between the results predicted by FLUENT and XFOIL with the same Reynolds number for the NACA0015 hydrofoil, whereas for the NACA0018-45 hydrofoil, a bigger lift, drag and pressure coefficient are predicted by FLUENT with the small limited domain compared with XFOIL, and it appears that the separation is retarded by the wall effect. Comparable lift coefficient and pressure distribution are obtained by an enlargement of the calculation domain which will weaken the wall effect. The values of the integrated forces of the NACA0018-45 hydrofoil predicted by FLUENT with different domain and XFOIL are listed in Table 2.

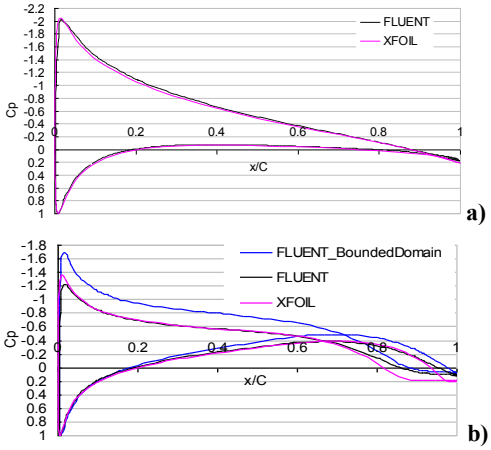

Figure 2: The pressure distribution along the (a)NACA0015 hydrofoil; and (b) NACA0018-45 hydrofoil as computed with FLUENT and Xfoil

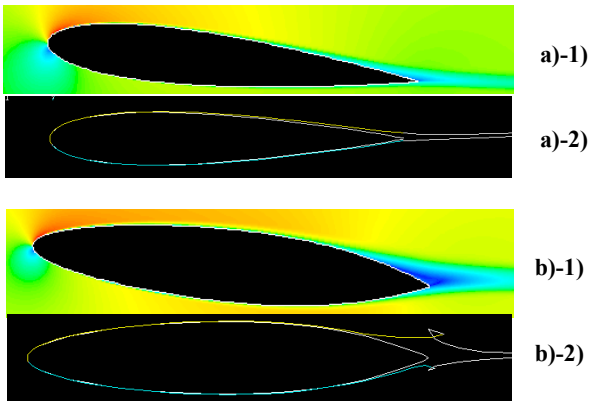

Figure 3: Contours of velocity magnitude (1) and the streamlines (2) for two different foils: (a) NACA0015 hydrofoil; and (b) NACA0018-45 hydrofoil, clearly showing the difference in separation zone

Table 2: Flow characteristics for NACA0018-45 hydrofoil

	FLUENT_Bounded Domain	FLUENT_Big Domain	XFOIL
CL	0.4990145	0.332673278	0.3314
CD	0.01780162	0.024103572	0.01267
Cpmin	-1.690956	-1.245765	-1.3717

3.2 2D Unsteady Cavitating Condition

Previous simulation results (LI Daqing et al 2009, Oprea et al 2009) show that unsteady dynamics with cyclic cloud cavity shedding would be observed for the NACA0015 hydrofoil at cavitation number equal to 1.0. Therefore, it can be assumed that the cavitating flow over the NACA0018-45 hydrofoil at the same cavitation number $\sigma = 1.0$ will show more intense unsteady dynamics due to its stronger pressure gradients under non-cavitating condition.

3.2.1 Unsteady Phenomena on NACA0015

The expected unsteady cyclic shedding has not been attained when the standard $SST\ k-\omega$ is adopted, confirming the lack of compliance with physics for the prediction of the turbulent quantities (Reboud et al 1998, Li et al 2009). On the condition that the solutions are assured to be converged, some factors that possibly retard the break-up dynamics are further investigated before accepting the modification to the standard $SST\ k-\omega$ model. Therefore, the sensitivity for grid density, turbulence models, bubble number density and the higher order of temporal discretization scheme are further investigated. Upon close examination, unsteady shedding still cannot be simulated, and only a back and forth oscillating sheet cavity can be observed with a maximum length of 43%C and minimum length of 20%C (Fig. 4).

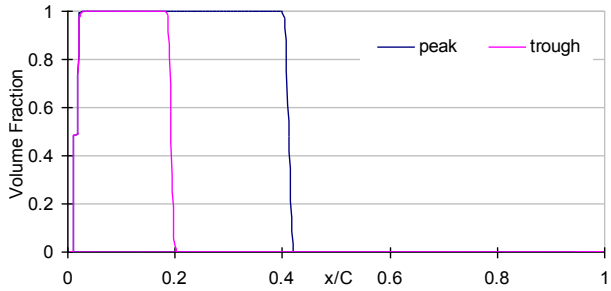

Figure 4: Volume fraction distribution over a NACA0015 hydrofoil at the peak and trough of the total vapor volume at $\sigma = 1.0$ with standard $SST\ k-\omega$ model

Based on the idea of Reboud et al to modify the standard $k-\varepsilon$ model (1998), an artificial reduction of the turbulence viscosity in the regions of higher vapor volume fraction is adopted on the $SST\ k-\omega$ model to study its capabilities for capturing the unsteady cyclic shedding phenomena. The test case is at first calculated with a time step size $\Delta t = 5e-04$ and 20 iterations per time step. It was found that this modified $SST\ k-\omega$ model can indeed predict the break-up of the sheet cavity and also the periodic shedding of the cloud cavity at the trailing edge of the sheet with a main natural frequency at 3.42 Hz, which is similar as the frequency reported by Li Daqing (2009) using FLUENT, as shown in Fig.5, but substantially differs from the 14 Hz reported by Oprea (2009) using StarCD and the 15.4 Hz reported by Hoekstra (2008) using ReFreSCo.

It is supposed that the discrepancy of the predicted frequency by FLUENT is related to the numerical uncertainties caused by an incomplete convergence. Therefore, a study of the influence of the time step size Δt and iteration numbers per time step I_N on the shedding frequency is conducted. It is suggested that the residuals should reduce by around three orders of magnitude within one time step to ensure accurate resolutions of transient behavior (Ferziger 2002). Apart from this criterion, a converged mass transfer rate for each time step can be used as a double check.

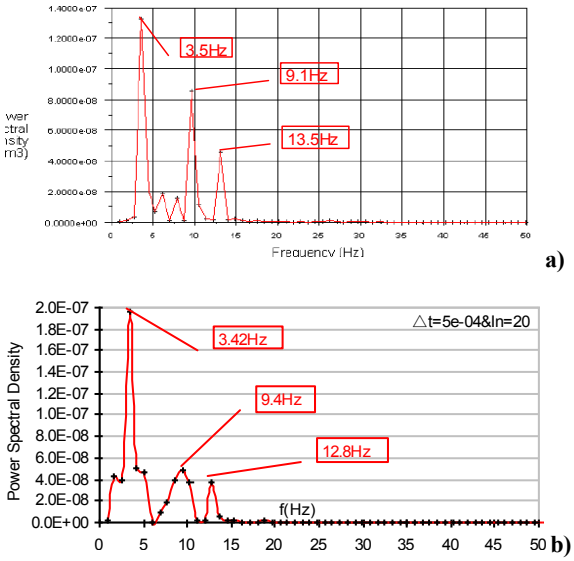

Figure 5: Shedding frequencies based on the vapor volume predicted by (a) Li Daqing (2009); and (b) current study

Figure 6 shows the behavior of residuals and mass transfer rate during one time step. It is found that the default number of 20 iterations is obviously inadequate to meet the convergence criteria. It is also found that more than 100 iterations are demanded to satisfy the three order reduction, but this may lead to numerical instabilities which may result in a sudden divergence during the entire simulation. Alternative test cases are conducted with another time step size $\Delta t = 1e-04$, where it is proposed that 50 iterations are already sufficient to achieve the convergence criteria, see Fig.7.

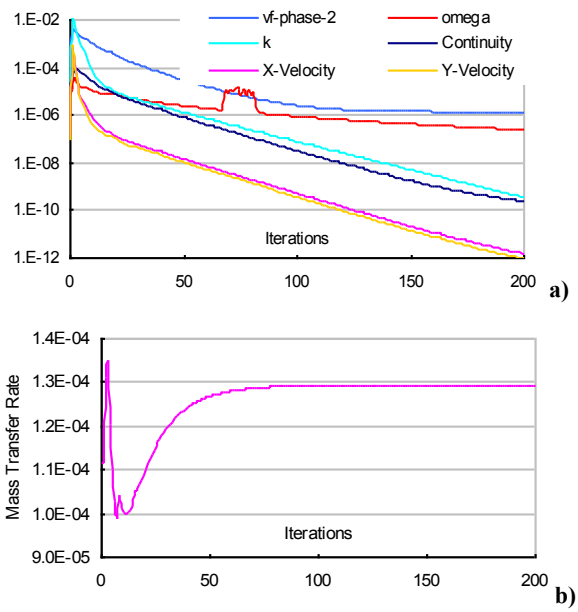

Figure 6: Behavior of the residuals (a) and mass transfer rate (b) during one time step $\Delta t = 5e-04$

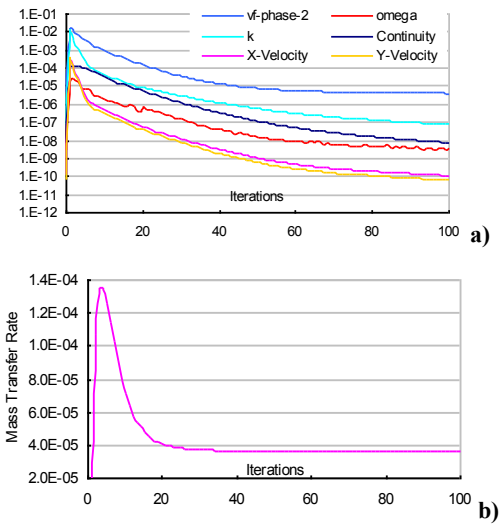

Figure 7: Behavior of the residuals (a) and mass transfer rate (b) during one time step $\Delta t = 1e-04$

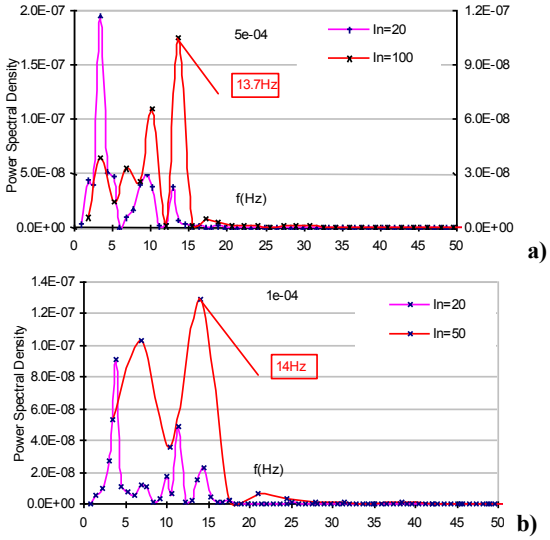

Figure 8: Shedding frequencies based on an FFT analysis of the integrated vapor volume with different I_N at (a) $\Delta t = 5e-04$; and (b) $\Delta t = 1e-04$

After an FFT analysis of the results, it is found that more adequate iterative solutions indeed show a preferable cyclic shedding at a more appropriate frequency, see Fig. 8. The main natural frequency increases to around 14 Hz, and more repeatable cyclic phenomena are observed.

The images shown in Fig. 9, which is predicted with $\Delta t = 5e-04$ and $I_N = 100$, clearly show the essential features of the unsteady shedding in a typical cycle. At first, a sheet cavity is growing from the leading edge after last cavity pinch-off (see Fig. 9 a)); a re-entrant jet forms subsequently and moves towards to the leading edge (Fig. 9 b)); The sheet cavity is then broken up by the re-entrant jet (Fig. 9 c)); The upstream part of the sheet cavity decrease to a very tiny volume, whereas the downstream part rolls up and transforms into a bubbly cloud (Fig. 9 d) and e)); Finally, the cloud cavity is lifted from the foil surface and collapses downstream in the vicinity of the trailing edge. Then a tiny sheet cavity from the leading edge grows again and a new cycle starts (Fig. 9 f)).

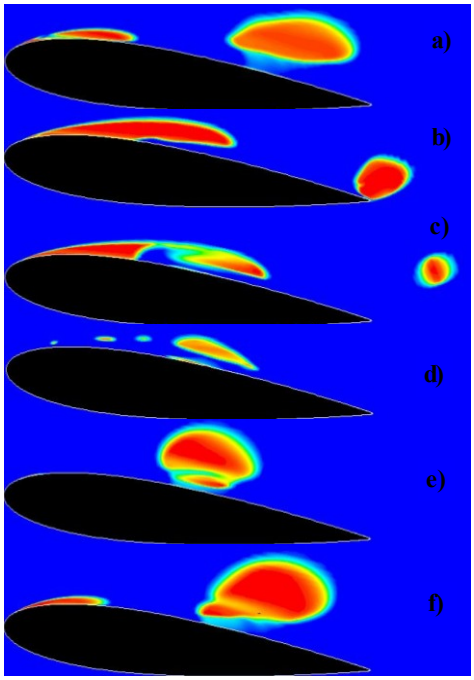

Figure 9: Contours of the vapor volume predicted by $\Delta t = 5e-04$ & $I_N = 100$ over a NACA0015 hydrofoil in one typical cycle

3.2.2 Unsteady Phenomena on NACA0018-45

Similar to the NACA0015 foil, the NACA0018-45 also shows a back and forth oscillating behavior when the turbulence model is not modified, see Fig.10. However, when it goes to the maximum volume, an initial re-entrant jet can be observed near the closure region of the cavity, as shown in Fig.11.

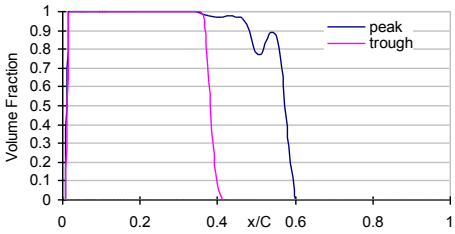

Figure 10: Volume fraction distribution over a NACA0018-45 hydrofoil at the peak and trough of the total vapor volume at $\sigma = 1.0$ with standard $SST\ k-\omega$ model

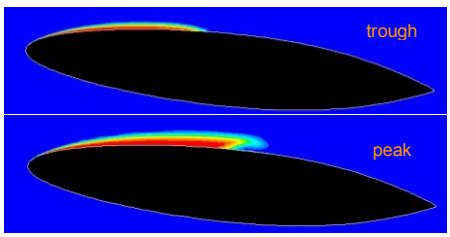

Figure 11: Contours of the vapor volume fraction at typical peak and trough of the total vapor volume at $\sigma = 1.0$ with standard $SST\ k-\omega$ model over a NACA0018-45 hydrofoil

Once the modified $SST\ k-\omega$ model is applied, a more typical and high-frequency cyclic shedding can be observed. The essential unsteady features, such as the break-up of the sheet cavity by the re-entrant jet and cloud cavity shedding, are similar to the NACA0015 hydrofoil,

as shown in Fig. 12. What is dissimilar is that there is a sheet cavity developing from the mid chord at the pressure side (see Fig. 12 d) and e)), which is consistent with the characteristic pressure gradient under the non-cavitating condition. Additionally, the cavity at the pressure side also collapses downstream near the pressure side trailing edge, and at the same time, another sheet cavity develops from the leading edge at the suction side, shedding a small cloudy cavity, and collapsing downstream (see Fig.12 e)-g)). This typical behavior is comparable with the experimental instantaneous photos shot by Foeth (2008) (see Fig. 13).

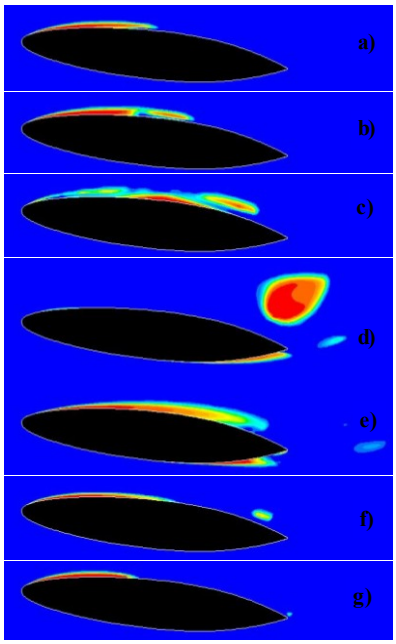

Figure 12: Contours of the vapor volume over a NACA0018-45 hydrofoil in one typical cycle

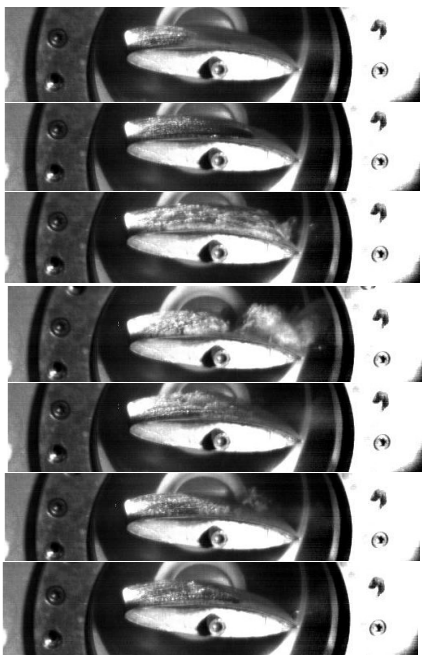

Figure 13: Sequence of experimental instantaneous photos during a typical cycle for the cavitating flow over a NACA0018-45 hydrofoil

3.2.3 Conclusions

The numerical issues, such as the time step size Δt and iteration numbers per time step I_N are shown to have an influence on the prediction of the unsteady break-up phenomena of the sheet cavity. The insufficient number of iterations can cause an inaccurate prediction of the shedding frequency and the magnitude of the total vapor volume. It is therefore important to check the numerical accuracy in advance so as not to affect the final assessment of the cavitation erosion risk.

3.3 3D Unsteady Cavitating Condition

3.3.1 Unsteady Phenomena on 3D NACA0015 hydrofoil

The test case is conducted on a 3D NACA0015 hydrofoil geometry, which is obtained by extruding the 2D mesh in the span-wise direction by 1.25 chord length. The boundary conditions on the two additional walls are set to symmetry conditions. Due to the complexity of 3D dynamics, there is no clear frequency obtained from the FFT analysis. However, the typical instants can be observed by visualizing the iso-surface of the instantaneous volume fraction ($\alpha = 0.1$): the sheet cavity is broken up by the re-entrant jet (Fig.14 a),b)); cloudy cavities form and roll-up (Fig.14 c),d)) and finally collapse downstream, at the same time the leading edge sheet cavity regrows and a new cycle starts (Fig.14 e),f)).

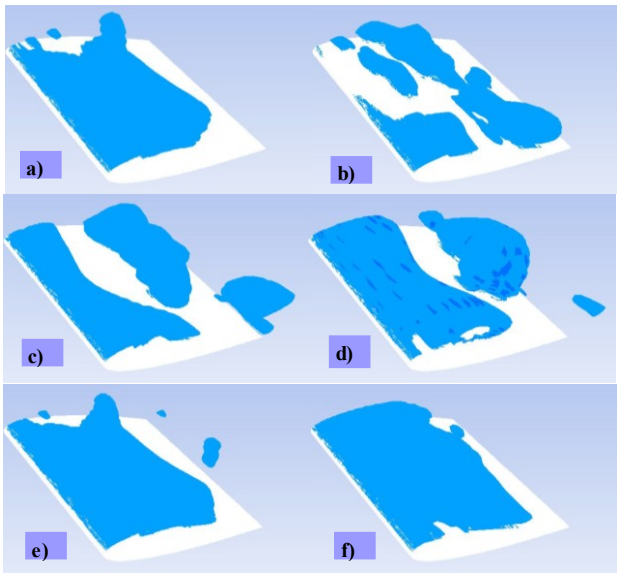

Figure 14: Sequence of iso-surface plots of the instantaneous volume fraction ($\alpha = 0.1$) during one typical shedding cycle on the NACA0015 hydrofoil at $\sigma = 1.0$

3.3.2 Assessment of Cavitation Erosion Risk

From an energy consideration, it is suggested here that the focusing of potential energy in a macro cavity occurs through large scale vortices produced in the break-up region of sheet cavitation. The high values of the impact loads they may produce are supposed to be related to the impulsive pressure pulses produced during the collapse process. The contours of the instantaneous static pressure distribution on the suction side, corresponding to the instants depicted in Fig. 14, are given in Fig. 15. It is shown that high pressure impacts can be observed at the

regions framed by red lines, which are consistent with the location where cloudy cavities collapse. This evaluation of results offers a possibility to assess the risk of cavitation erosion by the pressure impacts on the foil surface during the whole collapse process.

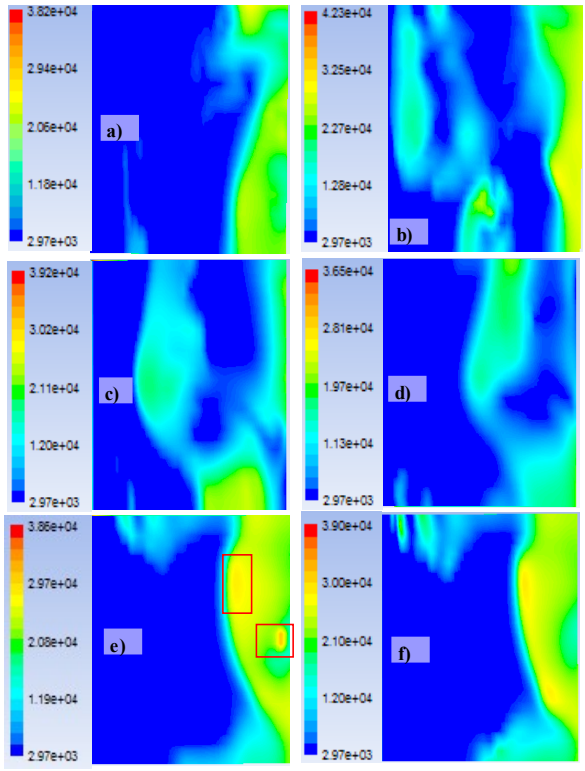

Figure 15: Sequence of contour plots of the instantaneous static pressure (in Pa) distribution on the suction side corresponding to each instant in Fig. 14

4 CONCLUSIONS AND RECOMMENDATIONS

The multiphase RANS code FLUENT is investigated on both a NACA0015 hydrofoil and a NACA0018-45 hydrofoil in order to assess its capability to capture the unsteady cavitating phenomena and subsequently the possibility to link the RANS results to the risk of cavitation erosion.

Some important conclusions are:

1. A realistic dynamic shedding of the sheet cavitation is only obtained after attenuating the eddy viscosity in the region with higher vapor volume fraction in the multiphase RANS code FLUENT. It is however noted that this eddy viscosity correction is not needed in all codes (see e.g. Oprea et al 2009, Hoekstra 2008).
2. The incomplete calculation for each time step may lead to an inaccurate prediction of the shedding frequency and the magnitude of the total vapor volume.
3. A tentative qualitative analysis on the correlation between the pressure impacts and the unsteady phenomena gives promise to an assessment of the locations where cavitation erosion may occur. Further validation of the locus of damage is however needed.

It is concluded that a reliable prediction of cavitation erosion is currently not directly possible with RANS codes, partly because of a lack of confidence in the prediction of even the large scale cavity dynamics, and partly because of a lacking procedure for an interpretation of results. An additional model using RANS results as input and providing more details on the collapse mechanism may be needed to provide a more quantitative criterion, such as the cloud collapse model as proposed by Wang & Brennen (1999). Further research in this direction is recommended.

REFERENCES

ANSYS FLUENT. (2009). ANSYS FLUENT 12.0 Theory Guide.

Bark, G., Berchiche, N. & Grekula, M. (2004). Application of Principles for Observation and Analysis of Eroding Cavitation – The EROCAV Observation Handbook. ed. 3.1.

Ferziger, J. H. & Peric, M. (2002). Computational Methods for Fluid Dynamics. 3rd ed. Springer.

Hoekstra, M, & Vaz, G. (2008). 'FreSCo Exercises for NACA0015 Foil'. VIRTUE WP4-Workshop II, INSEAN, Rome, Italy.

Hoekstra, M, & Vaz, G. (2009). 'The Partial Cavity on 2D Foil Revisited'. Proc. of the 7th Int, Symp. On Cavitation, Ann Arbor, Michigan, United States.

Li, D.Q., Grekula, M. & Lindell, P. (2009). 'A modified $SST\ k-\omega$ model to predict the steady and unsteady sheet cavitation on 2D and 3D hydrofoils'. Proc. of the 7th Int, Symp. On Cavitation, Ann Arbor, Michigan, United States.

Ligtelijn, J.Th. (2010). 'The Pay-off Between Cavitation and Efficiency'. IMarEST Ship Propulsion Systems Symposium, London, U.K.

Drela, M. & Youngren, H. (2001). XFOIL 6.9 User Guide.

Menter, F. R. (1994). 'Two-Equation Eddy-viscosity Turbulence Models for Engineering Applications'. AIAA Journal **32**(8), pp. 1598-1605.

Oprea, I. & Bulten, N. (2009). 'RANS simulation of a 3D sheet-vortex cavitation'. Proc. of the 7th Int, Symp. On Cavitation, Ann Arbor, Michigan, United States.

Reboud, J. L., Stutz, B. & Coutier, O. (1998). 'Two Phase Flow Structure of Cavitation Experiment and Modeling of Unsteady Effects'. Proc. of the 3rd Int. Symp. on Cavitation, Grenoble, France.

Schnerr, G. H. & Sauer, J. (2001). 'Physical and Numerical Modeling of Unsteady Cavitation Dynamics'. 4th Int. Conf. on Multiphase Flow, Orleans, United States.

Van der Hout, A. & Foeth, E. J. (2008). 'An Experimental Study on Cavitation Erosion on A Two-dimensional Hydrofoil'. TUDelft.

Van Terwisga, T. J. C., Fitzsimmons, P. A., Li, Ziru. & Foeth, E. (2009). 'Cavitation Erosion – A review of Physical Mechanisms and Erosion Risk Models'. Proc. of the 7th Int, Symp. On Cavitation, Ann Arbor, Michigan, United States.

Wang, Y. C. & Brennen, C. E. (1999). 'Numerical Computation of Shock Waves in a Spherical Cloud of Cavitation Bubbles'. Journal of Fluid Engineering **121**(2), pp. 872-880.